Chapter 4
The Structure and Stability of Simple Liquids

4.1 Introduction

In a recent paper Hagen *et al.* posed the question, 'Does C_{60} have a liquid phase?'[177] A liquid-vapour transition can only occur between the triple point temperature, below which only the solid and vapour are stable, and the critical temperature, above which there is only one fluid phase (Figure 4.1a). So, if the critical temperature is lower than the solid-fluid coexistence temperature at the critical density (Figure 4.1b), the liquid phase is thermodynamically unstable[178]. The answer to Hagen's question, though, has not yet been unequivocally answered: theoretical calculations of the phase diagram predict the liquid phase of bulk C_{60} is either unstable[177] or only marginally stable[179,180] depending on the simulation technique used, whilst experiment seems to suggest that C_{60} molecules are thermally unstable at the relevant temperatures[181].

In contrast to C_{60}, for which the intermolecular potential is very short-ranged with respect to the equilibrium pair separation, the critical temperature for sodium is about seven times larger than the triple point temperature because of the long-ranged interatomic forces. The results for C_{60} have led to a flurry of studies examining the effect of the range of the potential on the phase diagram[182–185]. These investigations have clearly shown that as the range of attraction decreases, the difference between the triple and critical temperatures decreases until the critical temperature drops below the triple point and the liquid phase disappears. Similar effects have previously been noted for mixtures of spherical colloidal particles and non-adsorbing polymer by theory[120], simulation[186] and experiment[121–123]. For such systems, the size of the polymer can be used to vary systematically the range

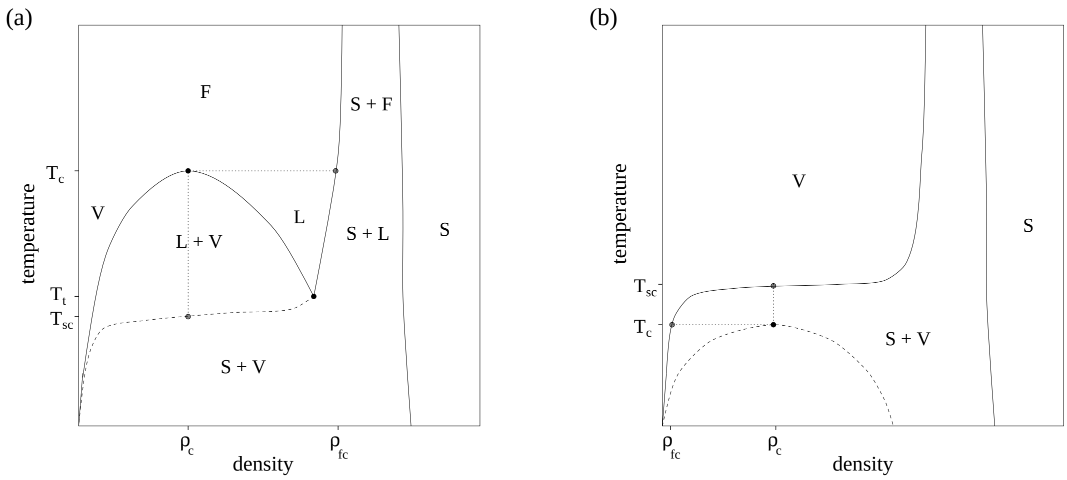

FIGURE 4.1: Temperature/density phase diagrams when (a) there is a stable liquid phase, and (b) the liquid phase is thermodynamically unstable. S, L, V and F stand for solid, liquid, vapour and fluid, respectively. T_c is the critical temperature, T_t is the triple point temperature, T_{sc} is the solid-fluid coexistence temperature at the critical density, ρ_c is the critical density, and ρ_{fc} is the density of the fluid which coexists with the solid at the critical temperature. The dashed lines are in (a) the metastable solid-fluid coexistence line and in (b) the metastable liquid-vapour coexistence line. For (a) $T_c > T_t > T_{sc}$ and $\rho_c < \rho_{fc}$ and for (b) $T_c < T_{sc}$ and $\rho_c > \rho_{fc}$. The latter are the necessary and sufficient conditions for there to be no stable liquid phase. The dotted lines are to guide the eye.

of attraction between the colloidal particles.

Although the phenomenology of the range-dependence of the liquid phase stability is clear, a structural explanation has not been given. In this chapter we provide such a microscopic view by relating the above effects to fundamental changes in the topography of the PES (§4.3) and by making a detailed connection between these changes and liquid structure (§4.4). By studying both clusters and bulk we can address questions concerning the emergence of the phase-like forms of clusters and their evolution to the bulk limit. Detailed simulations of the thermodynamic properties of a 55-atom cluster (§4.5) confirm that our results can explain the range-dependence of the thermodynamics. We can also suggest an explanation for the transition from electronic to geometric magic numbers observed in the mass spectra of sodium clusters[53] (§4.6), showing that the simple approach we describe here can provide insight into a diverse set of phenomena.

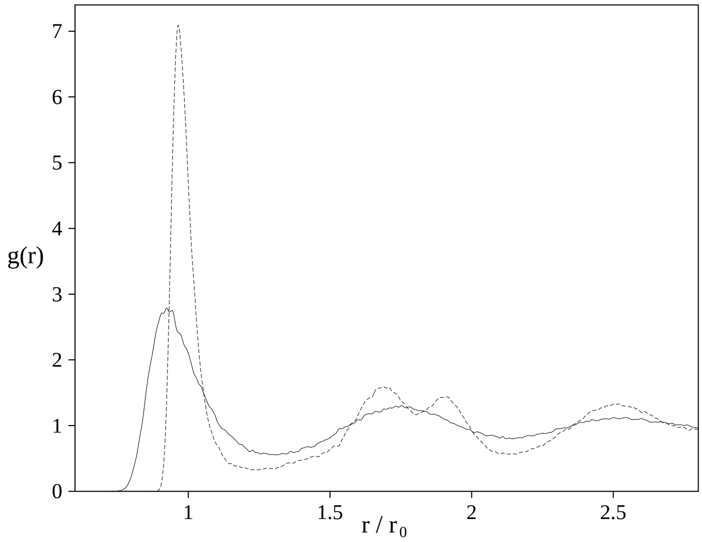

FIGURE 4.2: Bulk liquid radial distribution functions from a set of instantaneous coordinates (solid line) and the resulting minima after quenching (dashed line). The system is a periodically repeated cubic cell containing 256 atoms interacting via a Morse potential with ρ_0=6.

4.2 Methods

The focus of this chapter is to understand the dependence of the global topography (not just the low energy regions as in Chapter 2) of the PES on the range of the potential. To achieve this aim we again use the Morse potential; the analysis of the contributions to the potential energy given in §2.2.1 will be extremely important for understanding the range dependence of the thermodynamics.

In the present examination of the PES we will generally focus upon minima. As we noted in Chapter 3 this 'inherent structure' approach[148] allows one to analyse the thermodynamics in detail by separating the effects of the energetic distribution of local minima from the effects of thermal motion within the minima. Our analysis of the thermodynamics here will be more qualitative, simply concentrating on the distribution of minima. By removing the effects of vibrational noise this approach also allows a much clearer picture of liquid structure. This point is illustrated in Figure 4.2 by a comparison of the radial distribution functions derived from a set of instantaneous configurations of a bulk Morse liquid and the configurations of the corresponding minima. The peaks in the radial distribution function for the minima are much sharper, showing that the structure is much more well-defined. Of particular interest is the split second peak for the minima radial distribution function. This feature only develops in the instantaneous radial distribution function

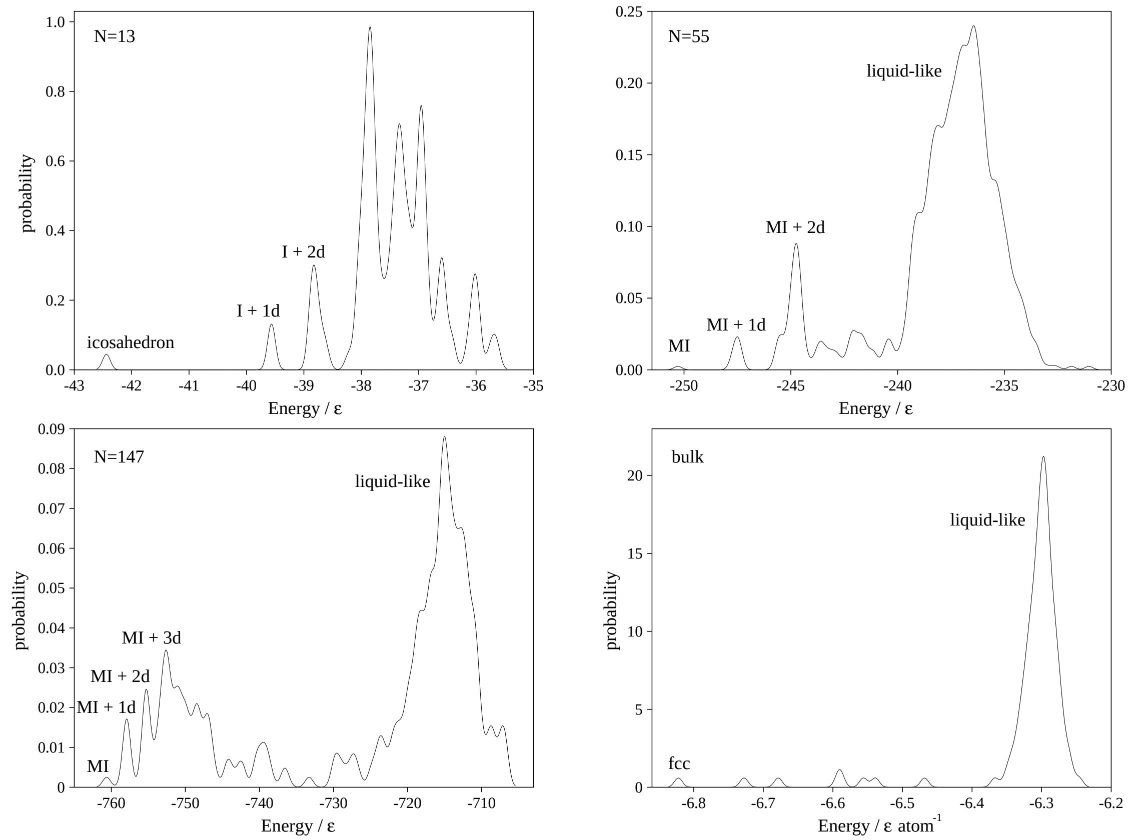

FIGURE 4.3: Probability distributions of the potential energy for samples of minima of M_{13}, M_{55}, M_{147} and bulk material. The samples contain 131, 858, 298 and 117 minima, respectively. Some of the peaks are labelled with the structures they correspond to. I stands for icosahedron, MI for Mackay icosahedron, $+\ n$d for a structure with n defects.

for supercooled liquids and glasses[187]. It is not too surprising that minimization and reducing the temperature have similar effects, and this helps to emphasize the structural connection between the liquid and the glass.

4.3 Correlation Diagrams

We employed molecular dynamics and conjugate-gradient techniques to generate between 10^2 and 10^3 local minima for each PES at $\rho_0 = 6$. The simulations of bulk material were performed at constant volume in a cubic box containing 256 atoms at a reduced density of $\sqrt{2}$. The three clusters we studied contained 13, 55 and 147 atoms, and have been chosen because they correspond to sizes for which complete Mackay icosahedra are possible. In the melting region these clusters fluctuate between a solid-like and a liquid-like state as a function of time. Consequently, a simulation at a single energy in this coexistence region was sufficient to sample

Table 4.1: Lowest energy minima found for M_{147}. The format is as for Table 2.2.

	PG	n_{nn}	E_{strain}	$\rho_0 = 3.0$	$\rho_0 = 6$	$\rho_0 = 10$	$\rho_0 = 14$	ρ_{min}	ρ_{max}
147A	C_1	729	97.629	**-1531.499**	-732.549	-637.693	-605.600		3.56
147B	I_h	696	26.896	-1509.272	**-760.631**	-678.171	-644.002	3.56	9.12
147C	C_s	674	1.514		-748.869	**-682.399**	-672.885	9.12	10.91
147D	C_s	674	1.495		-748.598	-682.386	**-672.911**	10.91	18.88
147E	C_{3v}	669	0.084	-1468.423[8]	-744.765	-678.962	-670.708	18.88	

all relevant regions of the PES's of the M_{13} and M_{55} clusters. However, for M_{147} separate simulations were needed to sample the equilibria between the solid and its low energy defective states, and between the high energy defective states of the solid and the liquid.

The four distributions of minima obtained are shown in Figure 4.3. The geometries of the local minima were subsequently reoptimized for ascending and descending integer values of ρ_0. For the bulk material, the box size was scaled at each value of ρ_0 to keep the energy of the fcc minimum at a constant fraction of its zero-pressure energy. On changing ρ_0 a minimum may disappear from the PES. When this occurs, geometry optimization leads to a new minimum and this causes the discontinuities in the correlation diagrams (Figure 4.4). This effect is particularly noticeable for the 13-atom cluster at long range, because the total number of minima on the PES at ρ_0=3 is less than the number of minima in our sample from ρ_0=6 (Table 2.1).

The lowest energy line in each correlation diagram at any given ρ_0 corresponds to the solid phase, since at zero Kelvin this structure must have the lowest free energy. For the bulk material (Figure 4.4), the lowest energy minimum is fcc for all values of ρ_0. However, as we saw in Chapter 2 the structure of the global minimum depends on ρ_0 for clusters. The global minima of M_{147} are illustrated in Figure 4.5, and their energies and the ranges of ρ_0 for which they are the global minima are given in Table 4.1.

In the correlation diagrams the relative slope of two lines is a measure of the difference in strain energies between two minima, a more positive slope implying a larger strain energy. For bulk material, the lowest energy lines above the fcc minimum are either close-packed structures misoriented with respect to the cubic box, or are based on the fcc minimum and contain defects such as vacancy-interstitial

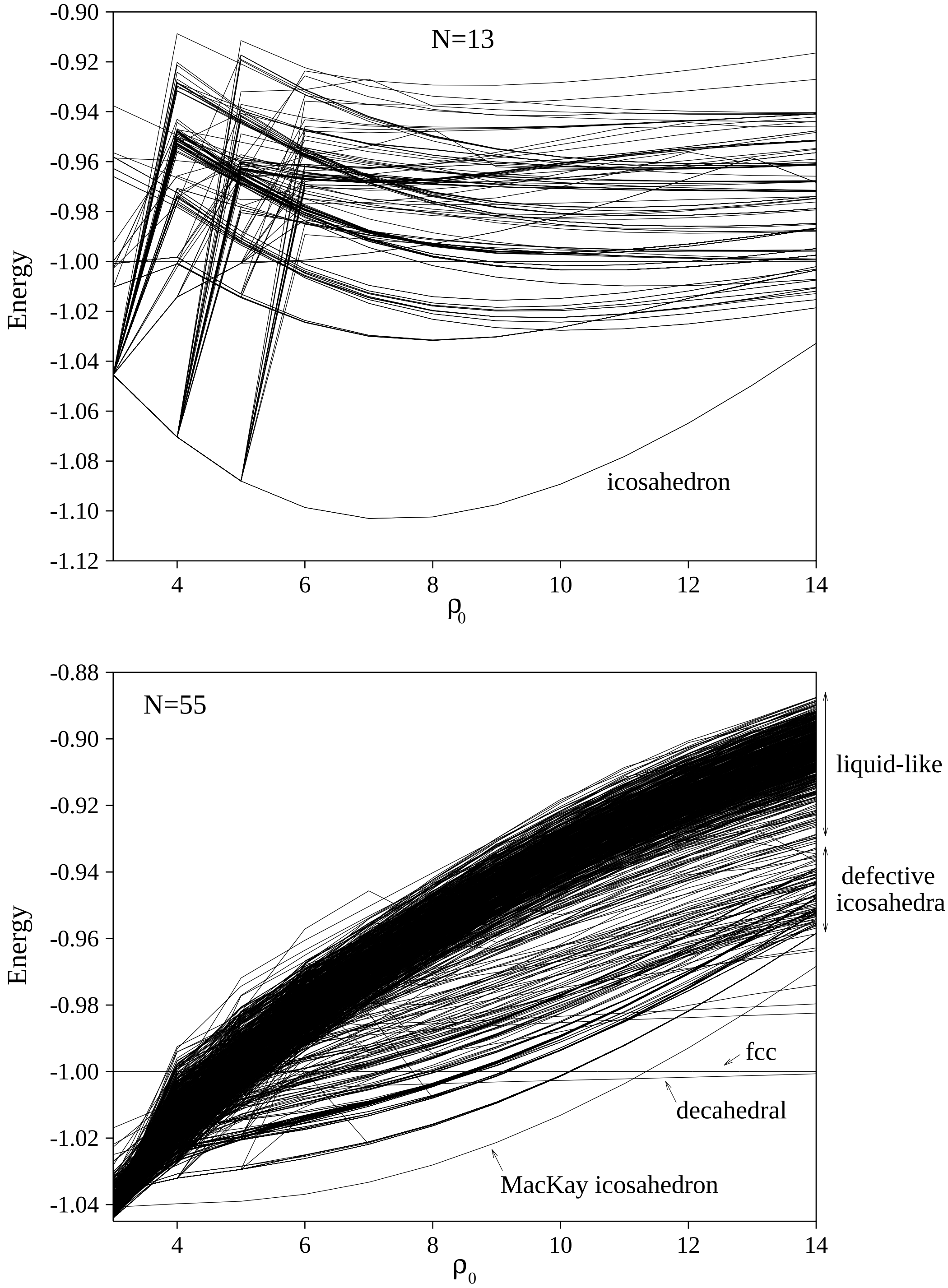

FIGURE 4.4: Correlation diagrams for M_{13}, M_{55}, M_{147} and bulk material. In each case the unit of energy is the binding energy of the lowest energy fcc structure. The samples contain 131, 858, 298 and 117 minima, respectively. Lines due to the decahedral and fcc structures which become the global minimum at large values of ρ_0 for M_{55} and M_{147} and the amorphous structure which is the global minimum of M_{147} at ρ_0=3 have been added.

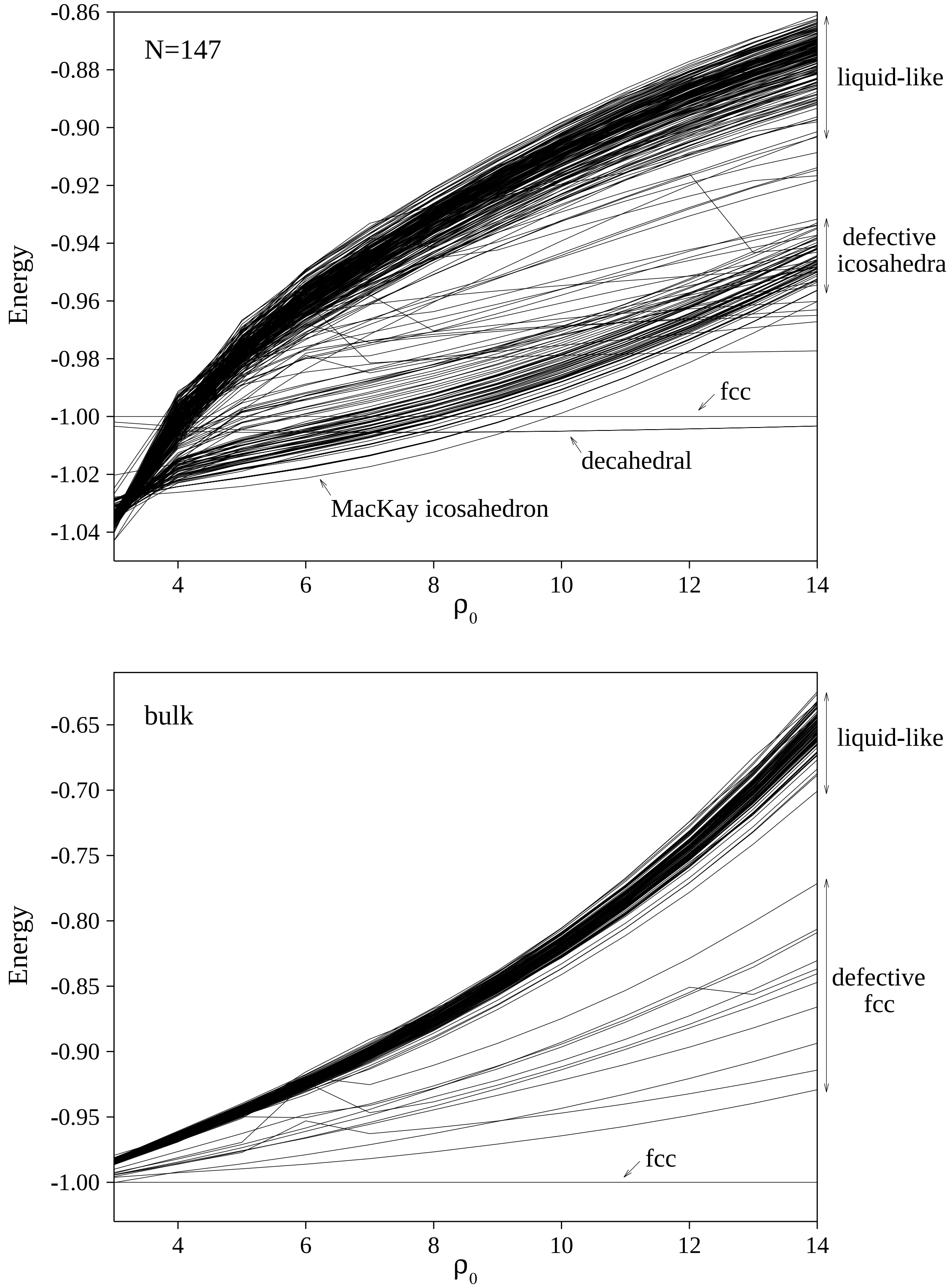

Figure 4.4: continued.

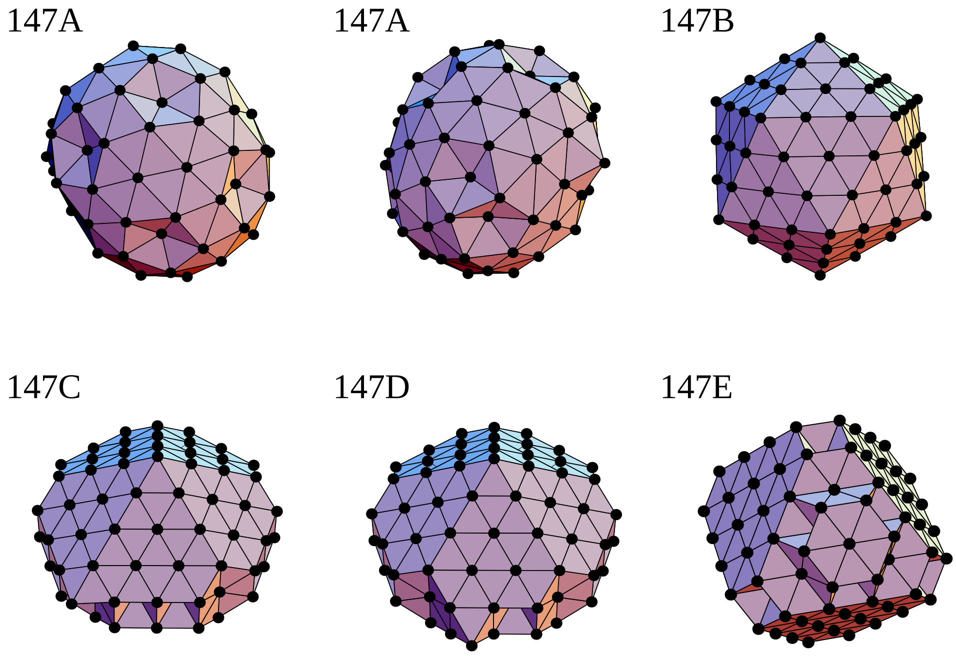

FIGURE 4.5: Global minima for M_{147}. Each structure is labelled by the symbol given in Table 4.1.

pairs. Both types of structure have a positive slope with respect to the perfect fcc structure, in the first case because the structure has to be sheared in order to fit into the box, and in the latter case because the interstitial defects introduce local strains. Although vacancies could be accommodated without any strain, the constant number and volume constraints used in this study only allow defects to be generated in pairs.

In contrast, the low energy lines in the cluster correlation diagrams run parallel to the line due to the icosahedral global minimum—a sign of their structural similarity. These lines are due to icosahedra with vacancies in the surface layer and adatoms on the surface. These minima give rise to the roughly equally-spaced peaks in the low energy region of the M_{55} and M_{147} probability distributions in Figure 4.3, and correspond to increasing numbers of defects. Rearrangements between these structures occur at energies just below that required for complete melting, leading to enhanced diffusion in the surface layer[110,111].

The thick bands of lines with positive slope in the bulk, M_{55} and M_{147} correlation diagrams along with the corresponding large, high energy peaks in the potential energy distributions (Figure 4.3) are due to minima found by quenching

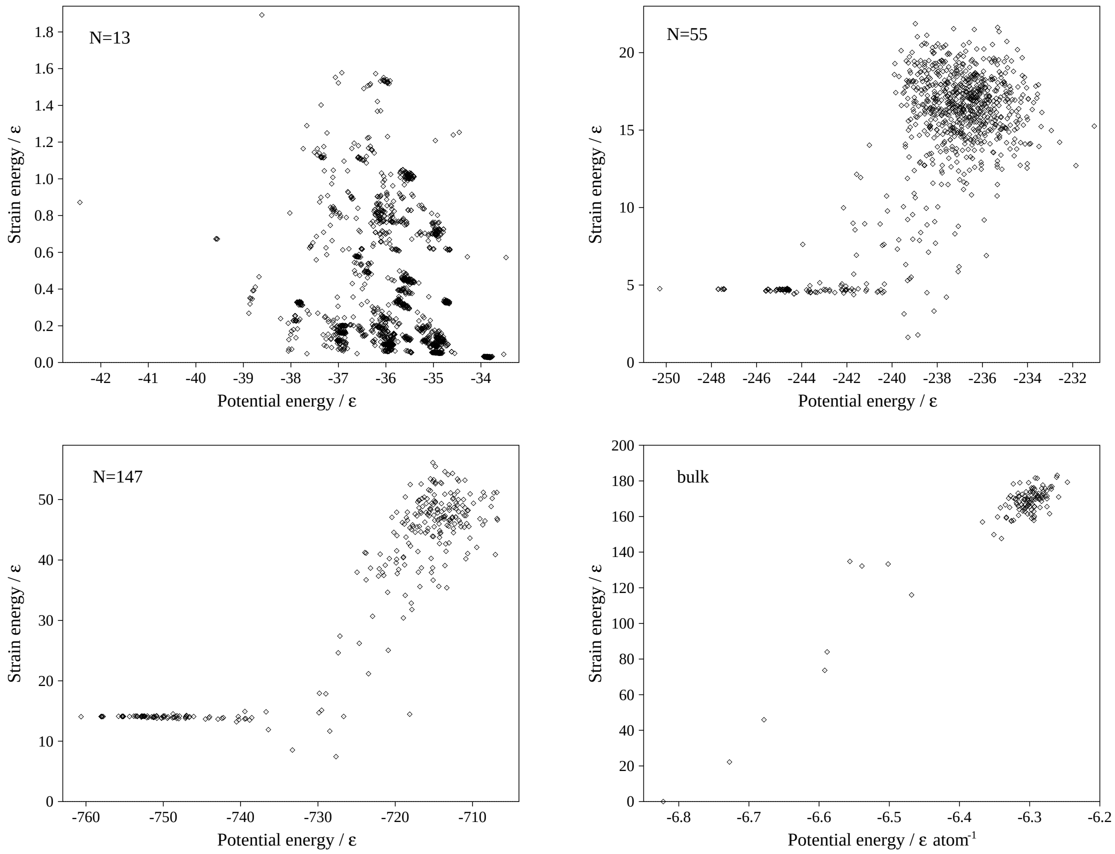

Figure 4.6: Plots of the strain energy versus the potential energy for the samples of ρ_0=6 minima for M_{13}, M_{55}, M_{147} and bulk material. The sample of M_{13} minima is larger than that used in Figure 4.4 and contains 1441 minima (Table 2.1).

from the region of phase space corresponding to liquid behaviour. We have sampled only a tiny fraction of all these 'liquid-like' minima; for comparison, the number of minima corresponding to the liquid-like phase space of LJ_{55} has been estimated as 8.3×10^{11} (§3.6). It is because of this large configurational entropy and the greater vibrational entropy that the free energy of the liquid phase usually becomes lower than that of the solid phase as the temperature increases, leading to melting. For the bulk, the energy gap between these 'liquid-like' minima and the fcc minimum clearly increases with ρ_0 (Figure 4.4). Thus, decreasing the range of the potential energetically destabilizes the liquid phase. For the clusters the energy of the 'liquid-like' minima must be compared to the energy of the global minimum. As the decahedral and fcc structures which become global minima at short range were not obtained in the sample of minima at ρ_0=6, the lines due to these structures have been added to the correlation diagrams, although we have not added lines due to the many defective minima based upon them. Hence, a similar result to bulk

TABLE 4.2: Partitioning of the potential energy of the bulk phases into the different contributions of equation 2.1 at different values of ρ_0. The values for the liquid phase are averages over all the 'liquid-like' minima. All energies are given in reduced units per atom. The nearest-neighbour criterion, $x_0 = 0.243$, corresponds to the minimum between the first and second peaks of the radial distribution function.

phase	ρ_0	E	n_{nn}	$E_{\rm strain}$	E_{nnn}
solid	6	-6.822	6.000	0.000	-0.822
	10	-6.050	6.000	0.034	-0.097
	14	-5.958	6.000	0.042	-0.016
liquid	6	-6.292	6.103	0.657	-0.846
	10	-4.935	5.931	1.134	-0.138
	14	-3.859	5.925	2.100	-0.034

is seen for M_{55} and M_{147}, i.e. the energy gap between the 'liquid-like' minima and the lowest energy solid structure, be it icosahedral or decahedral, clearly increases as the range decreases (Figure 4.4).

The physical basis for this behaviour is simply the greater strain energy of the 'liquid-like' minima, as shown by their positive slope in the correlation diagrams. Figure 4.6 shows clearly the differentiation between the low potential energy, low strain energy minima and the high potential energy, high strain energy 'liquid-like' minima. This greater strain arises from the inherent disorder of the 'liquid-like' minima; they have a range of nearest-neighbour distances, and consequently the first peak in the radial distribution function is broader than for the solid. The strain energy is the energetic penalty for this disorder and it rises rapidly as the range decreases and the potential wells narrow. This view is confirmed by examining the three contributions to the energy for the two bulk phases at different values of ρ_0 (Table 4.2). The main contribution to the energy gap is found to be the larger strain energy of the liquid minima. This greater strain energy will be related to the liquid structure in more detail in §4.4.

The energetic destabilization of the liquid phase seen for bulk and the two larger clusters gives rise to a term in the free energy difference between the solid and liquid phases which increases rapidly with ρ_0. Since the energetics of the vapour phase can be assumed to be relatively unaffected by the range of the potential, the rise in energy of the 'liquid-like' minima with ρ_0 for bulk and the two larger clusters also causes the energy difference between the liquid and vapour to decrease. Thus, the range-dependence of the energetics should have a large effect on the free energy differences both between the solid and liquid phases and between the liquid and vapour phases, in both cases destabilizing the liquid phase. It is significantly harder to determine the range-dependence of the entropic contribution to the free energy in our approach. However, the entropy of the vapour phase should be relatively unaffected by ρ_0 and the entropy of both the solid and the liquid phases decreases as ρ_0 increases due to the narrowing of the potential wells and the attendant loss of accessible configuration space. We have shown that the range-dependence of the energetics is sufficient to account for the known range-dependence of the phase diagram and in particular the decrease of the critical temperature as the potential becomes more short-ranged. Thus, at least part of the destabilization of the liquid phase that has been noted in experiments and simulations of colloids and C_{60} can be traced to the PES in this way.

The situation for M_{13} is rather different because of its small size—this cluster is nearer to the atomic limit. The introduction of defects in the icosahedron involves an increase in the energy of the cluster which is a significant fraction of the total potential energy. The heat capacity peak found for LJ_{13} (it should exhibit very similar behaviour to an M_{13} cluster with $\rho_0 = 6$) is associated with isomerization between the icosahedron and the defective structures based upon it[128], rather than between two phase-like forms that are structurally dissimilar. The nature of the 'melting' transition is therefore significantly different from the larger clusters and from bulk. As the removal of an atom from the vertex of the icosahedron allows relaxation of some of the strain, the gap between the icosahedron and the defective states decreases as the range of the potential decreases.

There is another interesting effect evident in the correlation diagrams of M_{55} and M_{147}: as ρ_0 decreases the gap between the 'liquid-like' band of minima and the Mackay icosahedron decreases until for a sufficiently long-ranged potential the 'liquid-like' band becomes lower in energy than the icosahedron. At $\rho_0 = 3$ for both M_{55} and M_{147}, the lowest energy clusters (55A and 147A) have an amorphous structure typical of the liquid-like state, which as we saw in §2.3.4 can be analysed in terms of disclination lines.

4.4 Liquid Structure

In this section we relate our results to current models of the structure of liquids and glasses and perform further structural analysis on our samples of minima. Our investigations of clusters are particularly helpful in this task since models of liquid structure often make use of results from cluster studies[188–190]. It was Frank who first suggested that the large supercooling of atomic liquids might be due to a local icosahedral ordering in the liquid phase. He justified this suggestion by pointing out that for a 13-atom Lennard-Jones cluster the icosahedron was significantly lower in energy than the fcc cuboctahedron. It has since been demonstrated that the structure of atomic liquids and glasses has significant polytetrahedral character[191], first through the success of the dense random packing of hard spheres[192,193] as a model for metallic glasses[194] and later by computer simulations[195]. In this polytetrahedral model liquid structure is considered to be a tessellation of all space by tetrahedra with atoms at the vertices of the tetrahedra. The 13-atom icosahedral cluster is an example of a finite polytetrahedral structure as it is composed of twenty face-sharing tetrahedra. Local icosahedral arrangements are therefore possible, although not necessary, in bulk polytetrahedral packings.

One reason suggested for the polytetrahedral character of liquids is the fact that the regular tetrahedron represents the densest possible local packing of spheres. However, the regular tetrahedron cannot be used to pack all space. This is illustrated in Figure 2.3; if five regular tetrahedra are packed around a common edge, there remains a small gap of $7.36°$, and if twenty regular tetrahedra are packed around a common vertex the gaps amount to a solid angle of 1.54 steradians, which is equivalent to 2.79 additional regular tetrahedra. This incompatibility of the preferred short-range order with a global packing is termed 'frustration'. As a consequence of this frustration, close packing, which consists of a mixture of regular tetrahedra and octahedra, rather than a polytetrahedral packing, is the densest packing of all space. Furthermore, a polytetrahedral packing of space must involve tetrahedra that are distorted from regularity, leading to local strains and a range of nearest-neighbour distances. Polytetrahedral structure therefore underlies the larger strain energies in the liquid phase and the dependence of liquid stability on the range of the potential.

The radial distribution functions shown in Figure 4.7 provide evidence for the polytetrahedral character of the liquid minima through the absence of a peak at $r = \sqrt{2}$, which is the signature of the octahedra that occur in closed-packed

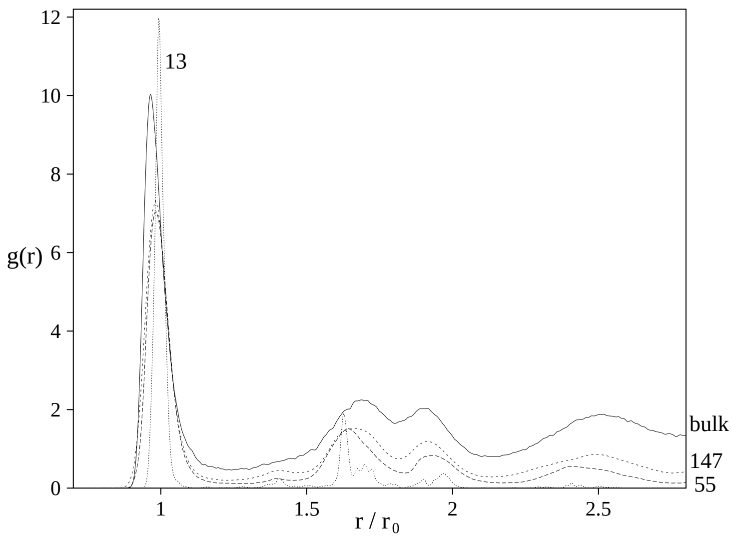

FIGURE 4.7: Average radial distribution functions, $g(r)$, for the four sets of 'liquid-like' minima at $\rho_0 = 6$. The distribution function has not been normalized with respect to the density since the volume of a cluster is not well-defined.

structures, and the split second peak. The split second peak of the structure factor, which is a common feature of supercooled liquids and glasses, has also been shown to be a consequence of polytetrahedral order[196].

We have also performed a common-neighbour analysis[149,195,197] for our samples of minima. This analysis assigns four indices $ijkl$ to each pair of atoms which have common neighbours, and provides a description of the local environment of the pair. Firstly, those pairs of atoms which are separated by less than a physically reasonable cutoff distance are designated nearest neighbours. We have simply set the cutoff equal to the minimum between the first and second peaks in the liquid radial distribution function. For those pairs of atoms which are nearest neighbours i is assigned the value 1. For those pairs of atoms which are not nearest neighbours but which have common neighbours i is assigned the value 2. The index j specifies the number of neighbours common to both atoms. The index k specifies the number of nearest-neighbour bonds between the common neighbours. The index l specifies the longest continuous chain formed by the k bonds between common neighbours.

This analysis allows differentiation between different types of local order. In particular, 1421, 1422 and 2444 (an octahedron) pairs are associated with close packing; 1555 (a pentagonal bipyramid), and 2333 (a trigonal bipyramid) pairs are associated with polytetrahedral packing. Scatter plots of some of these indices

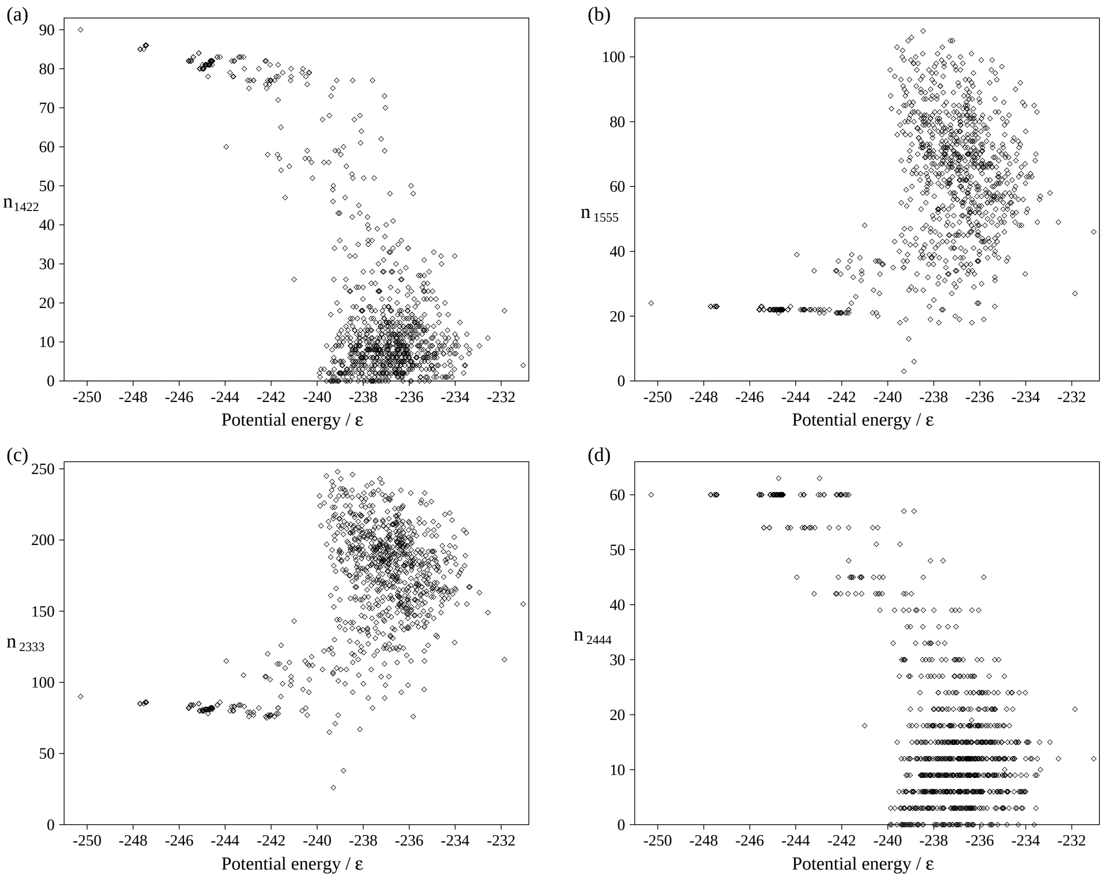

FIGURE 4.8: Scatter plots of the number of (a) 1422, (b) 1555, (c) 2333 and (d) 2444 pairs defined by the common neighbour analysis for the 858 M_{55} $\rho_0 = 6$ minima.

for the M_{55} minima are shown in Figure 4.8. The plots clearly show that the higher energy 'liquid-like' minima have a larger proportion of polytetrahedral pairs and fewer close-packed environments. Furthermore, a common neighbour analysis allows the properties associated with certain local environments to be found. In Figure 4.9, we decompose the second peak of the radial distribution function for M_{55} according to the types of common neighbour pairs. The first subpeak is clearly due to trigonal bipyramids (2333 pairs) and the 2nd subpeak to linear configurations (2100 pairs). The split second peak is therefore an indicator of polytetrahedral order. The effect of 2111 pairs (a pair of atoms at the apices of a rhombus) is smaller than in the case of bulk hard sphere systems[197].

The constraints that lead to the frustration inherent in polytetrahedral packings of 3-dimensional Euclidean space can be altered by introducing curvature into the space. In fact, in a space of appropriate positive curvature a perfect tetrahedral packing can be achieved in which there is no frustration and each atom

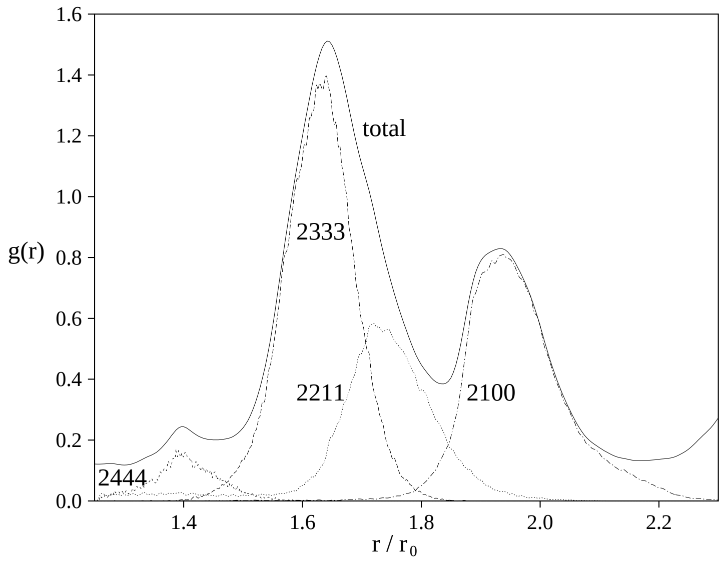

FIGURE 4.9: Decomposition of the second peak of the radial distribution function of M_{55} $\rho_0 = 6$ 'liquid-like' minima by common neighbour analysis. The solid line is the total radial distribution function and the dashed lines are the components due to four types of common neighbour pairs as labelled.

is icosahedrally coordinated. The resulting structure is that of polytope $\{3,3,5\}$ which consists of a regular arrangement of 120 atoms on the 3-dimensional hypersurface of a 4-dimensional hypersphere[198,199]. The effects of this lack of frustration have been well illustrated in work by Straley[200,201] who compared the melting and crystallization of an fcc crystal in flat space, with that of polytope $\{3,3,5\}$. In particular, the kinetics of crystallization from a liquid are much easier on the 4D hypersphere. In line with Frank's original suggestion concerning the supercooling of metallic liquids, this result has been interpreted as showing that the solid and liquid on the 4D hypersphere have the same kind of order, i.e. both are polytetrahedral. Therefore, it provides further evidence for the polytetrahedral nature of the liquid phase.

Nelson has shown that in the transformation of regular polytetrahedral packings from curved to Euclidean space disclination lines must be introduced[198,199]. If these disclination lines are arrayed periodically one obtains crystalline structures called Frank-Kasper phases[202,203]. If the disclination lines have a disordered arrangement it has been suggested that one obtains structures typical of liquids and glasses. The disclination networks for three types of Frank-Kasper phase, termed the A15, C15 and T phases[204], are illustrated in Figure 4.10; the disclinations of the T phase form an interconnected network of dodecahedra. The Frank-Kasper phases

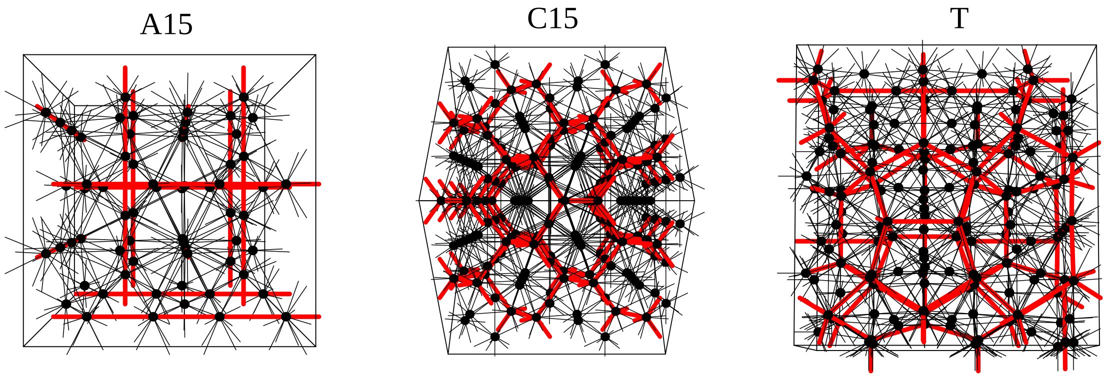

Figure 4.10: Some examples of the ordered arrays of disclination lines that occur in Frank-Kasper phases: A15, e.g. β-W, C15, e.g. $MgCu_2$, and T, e.g. $Mg_{32}(Zn,Al)_{49}$. The $-72°$ disclination lines are indicated by thick red lines. Disclination-free nearest-neighbour bonds are indicated by thin black lines.

are sometimes referred to as tetrahedrally close-packed because of their polytetrahedral nature and are closely related to many icosahedral quasicrystals[205]. The known examples are generally alloys where some of the frustration is relieved by the different atomic sizes. It has been suggested that a mixture of different-sized fullerenes might be able to form a Frank-Kasper phase and even quasicrystals[206]. However, this seems unlikely given the short-ranged character of fullerene potentials (§2.2.1)—the structures must still be able to accommodate some strain. Interestingly, the dual of the A15 Frank-Kasper phase (Figure 4.10) has recently been found to divide space into equal cells of minimum surface area[207], overturning Kelvin's proposed optimal structure[208] which stood for over a century.

On the unfrustrated 4D hypersphere there must be an equal number of positive and negative disclinations. However, as a consequence of the residual gap that occurs when five regular tetrahedra share a common edge in Euclidean space (Figure 2.3a), there must be an excess of negative disclinations[198,199]. For example, the Frank-Kasper phases involve only negative disclinations (Figure 4.10). If an atom is 12-coordinate by the Voronoi procedure, it can be free of disclinations. However, atoms that have a different coordination number must have disclinations passing through them. Using Euler's rule and the fact that the coordination polyhedra are deltahedral, one can deduce the coordination polyhedra which involve the minimum number of disclinations. These polyhedra are termed the Kasper polyhedra, and are illustrated in Figure 4.11. (They are denoted by ZN, where N is the coordination number.) For example, apart from icosahedra the A15 Frank-Kasper phase (Figure 4.10) involves only Z14 Kasper polyhedra, and the C15 structure

(Figure 4.10) involves only Z16 Kasper polyhedra.

We can also understand the range-dependence of the energy of the 'liquid-like' minima by considering the energetics of disclination lines. The strains associated with the disclination lines are most easily accommodated in systems bound by long-ranged forces. In fact the clusters which correspond to the Kasper polyhedra Z10, Z13, Z14 and Z15 are the global minima for the Morse potential at $\rho_0 = 3$, and those that correspond to Z11 and Z16 are the second lowest energy stationary points of their size (§2.3.4). As the range of the potential decreases the energetic penalty for the local strains associated with the lines increases, causing destabilization of the liquid phase.

In Nelson's original paper outlining his disordered disclination model for liquid structure, he gives a schematic diagram of such an arrangement[198,199]. The sketch involves only Kasper polyhedra; long disclination lines, mediated by the Z10 and Z14 Kasper polyhedra, thread through the icosahedrally coordinated medium, and the other Kasper polyhedra act as nodes for the disclinations. Surprisingly, no-one, as far as we are aware, has attempted to verify this model by visualization of the disclination network. However, results from the statistical analysis of Voronoi polyhedra indicate that the density of disclinations is higher than this picture would suggest; for example, in Finney's analysis of dense random packings of hard spheres only 40% of the faces of the Voronoi polyhedra are pentagonal, thus indicating that for this system about 60% of bonds involve disclinations including a significant number of 144°-type[209]. In part of Figure 4.12 we show the disclination network for a typical bulk liquid minimum; the disclination density is so high that the result is an unintelligible mass of lines. Typically, for the minima we analysed, only about 10% of the atoms have an icosahedral or Kasper polyhedral coordination shell, in contrast to Nelson's original picture. However, the disclination density is likely to be lower for simple binary liquids where the size of the atoms are chosen to reduce the frustration. It is for such a system that the most striking examples of local icosahedral order have been obtained[195].

As we saw in Chapter 2, the lowest energy structures of clusters at low ρ_0 are polytetrahedral. Furthermore, Figure 4.4 shows that for M_{55} and M_{147} these structures correlate with low energy liquid-like minima. Therefore, Figures 2.10 and 2.18 allow us to see how polytetrahedral packings and liquid structure evolve with size. At small sizes is it possible to accommodate the strain that is associated with the bridging of the 'gaps' that occur in a disclination-free packing of regular tetrahedra (Figure 2.3). Anti-Mackay growth on the 13-atom icosahedron gives

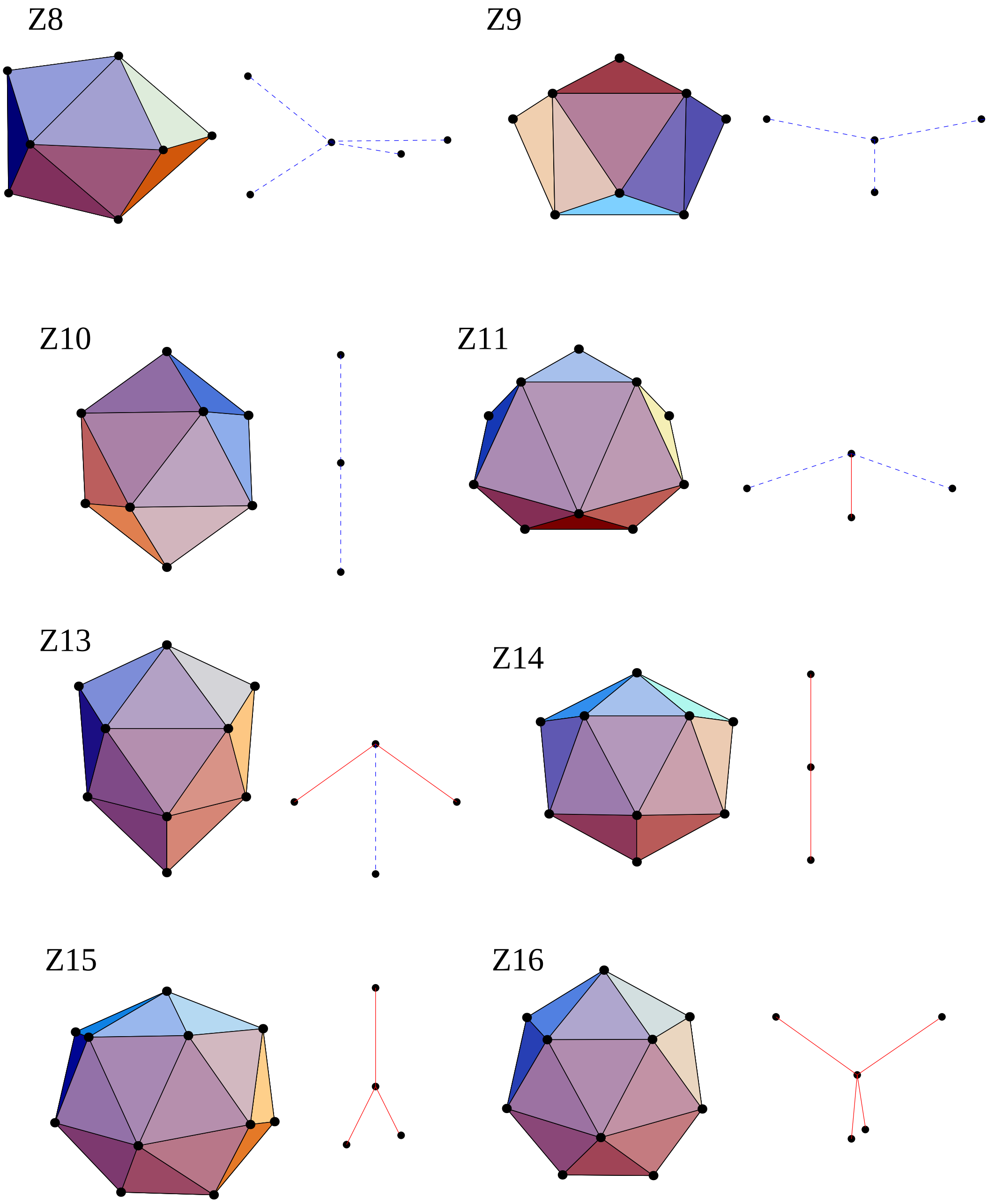

FIGURE 4.11: Kasper Polyhedra for coordination numbers between 8 and 16 (except for the disclination-free icosahedral coordination shell). Both the coordination polyhedra and the associated disclination lines are shown. Negative disclinations are represented by red lines and positive disclinations by dashed blue lines

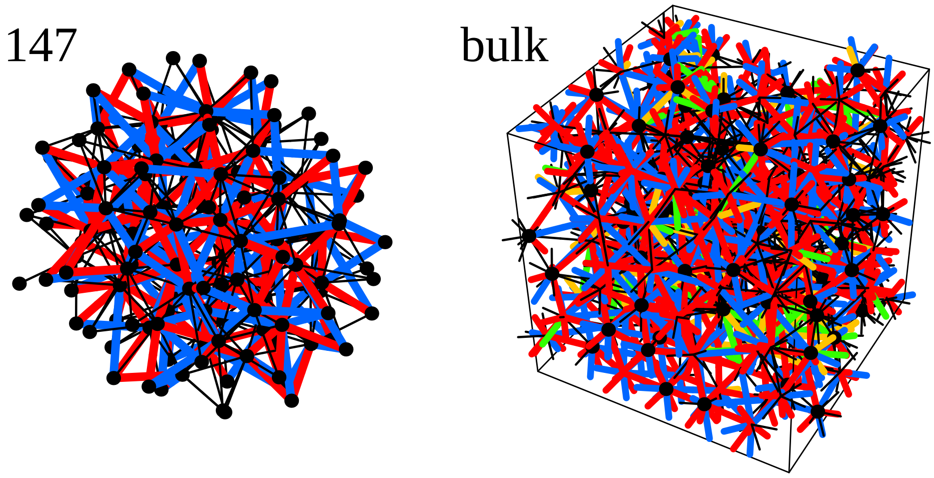

Figure 4.12: Disclination networks for the ρ_0=3 M_{147} global minimum and a bulk Morse liquid minimum. Thin black lines represent nearest-neighbour bonds which are disclination-free, red lines represent $-72°$ disclinations, blue lines $+72°$ disclinations, green lines $-144°$ disclinations, and yellow lines $+144°$ disclinations.

disclination-free polytetrahedral structures up to 45. Above this size disclinations have to be introduced. Whilst the disclination density is still small, ordered arrangements of the disclinations, which are fragments of Frank-Kasper phases, can form at some sizes (N=51–53, 56, 57, 59–61, 70, and 74). However, as the size increases the structures become progressively more disordered. By the time M_{147} is reached the cluster is a mass of interconnected disclinations (Figure 4.12); only 53% of the interior bonds of 147A are disclination-free.

Why should liquids have a polytetrahedral structure though? Why is liquid structure not more like a highly defective version of the solid? Stillinger and Weber have used a model partition function to show that if defects of a body-centred-cubic lattice interact, then a first-order melting transition can occur which is associated with the condensation of a 'gas' of defects[210]. One of the common reasons suggested for the polytetrahedral character of liquids is the energetic favourability of local icosahedral order. This argument dates back to Frank and his comparison of icosahedral and cuboctahedral 13-atom clusters that we mentioned above. However, this argument contains a fallacy. The reason for the lower energy of the icosahedron is primarily a surface effect; each surface atom is six-coordinate for the icosahedron and five-coordinate for the cuboctahedron. The actual energy of the interior atom will be slightly higher for the icosahedron, because the radial nearest-neighbour distance is slightly compressed with respect to the ideal. Furthermore, as has been pointed out by Clarke and Jonsson[197], an energetic argument cannot account for the fact that dense random packings of hard spheres (where all configurations have the same energy) show significant polytetrahedral order. Another observation is the fact that the tetrahedron has the greatest local density. However, if one considers the density of an icosahedron, the distortion required to bridge the gaps of Figure 2.3b leads to a decrease in density to such an extent that a cuboctahedron is denser[211].

What then is the reason for the polytetrahedral structure of liquids? To answer this question one needs to realize that polytetrahedral packings should be compared not to the close-packed solid, but to other states that could possibly mediate a melting transition. The number of ways of arranging disclination lines in a polytetrahedral packing or of introducing disclination lines into polytope $\{3, 3, 5\}$ to bring the curvature nearer to that of flat space is huge[212]. Consequently, there is a large configurational entropy associated with the set of all polytetrahedral states. Yet they are also fairly dense, and depending on the range of the potential, can be fairly low in energy. It is the combination of these three factors (or the first two in the case of hard spheres) which underlies the favourability of polytetrahedral order.

One of the fundamental questions of cluster science is when and how bulk-like character develops. The answer of course depends on the property considered. For instance, the structure of solid-like clusters only becomes bulk-like at large sizes for many systems, especially for those clusters with a long-ranged potential[213]—sodium clusters are icosahedral up to at least 20 000 atoms[53] even though the bulk structure is body-centred cubic. In contrast, our results show that bulk-like liquid structure can develop at rather small cluster sizes. This is suggested by the similar energetic destabilization of the bulk, M_{55} and M_{147} 'liquid-like' minima and by the clear similarity of their radial distribution functions (Figure 4.7). The only significant difference is the uniformly smaller value of the cluster radial distribution function, and this is simply due to the finite size. The peaks in the M_{13} radial distribution function are at a similar position to the larger clusters but are much sharper because at this size the effects of frustration are small. The similarity of bulk and cluster radial distribution functions can easily be understood within the polytetrahedral model of liquid structure. Given the favourability of polytetrahedral structure for small clusters and the rapid increase in disclination density with size, it is not surprising that bulk-like liquid character is seen at small sizes.

As the size of the Mackay icosahedron increases, the polytetrahedral character decreases and the close-packed character increases. This can explain some of the differences in the correlation diagrams of the two larger clusters (Figure 4.4). For the 55-atom cluster the distinction between the top of the band of defective icosahedral structures and the band of 'liquid-like' minima is unclear because of the greater structural similarity of the solid and the liquid at this small size. The energetic separation of these two bands of minima becomes larger as the number of atoms increases, giving the correlation diagram of M_{147} the two-state character expected for a system that undergoes a first-order phase transition.

Another related effect is the energetic differentiation between the minima found by quenching from a glass or supercooled liquid and from the liquid that occurs for M_{147}. Structure 147A (Figures 4.5 and 4.12), the global minimum at $\rho_0 = 3$, was found from the collapse of one of the 'liquid-like' minima of our sample. It can be seen in Figure 4.4 that at $\rho_0 = 3$ there is an energy gap between this and the next lowest energy minimum that we found. This is not because there are no minima in between. In fact, we found that this gap was an artifact of our sample; 147A is actually at the bottom of a band of minima which is almost continuous in energy. The clue to the nature of structure 147A came when it was reoptimized for ascending values of ρ_0; the resulting line runs parallel to but below the main 'liquid-like' band, indicating that it is of essentially similar structure to the 'liquid-like' minima. This suggested that 147A was one of a set of minima that for a medium-ranged potential comes from a glassy region of phase space; these states are essentially just the low energy continuation of the 'liquid-like' band of minima but are never observed at equilibrium because of their smaller entropy. This hypothesis was confirmed by quenching from a supercooled M_{147} liquid at $\rho_0 = 6$. The resulting minima were lower in energy than the 'liquid-like' band, but as for 147A ran parallel to the 'liquid-like' band in the correlation diagram.

4.5 The 55-atom Morse Cluster

In this section we shall illustrate the effects of the range of the potential on cluster thermodynamics in more detail, by presenting results of simulations of M_{55} at different values of the range parameter, ρ_0. As in §3.3 we use STA temperature distributions (e.g. Figure 4.13) to decompose the caloric curve into contributions from different states. The caloric curves for M_{55} at five different values of ρ_0 are

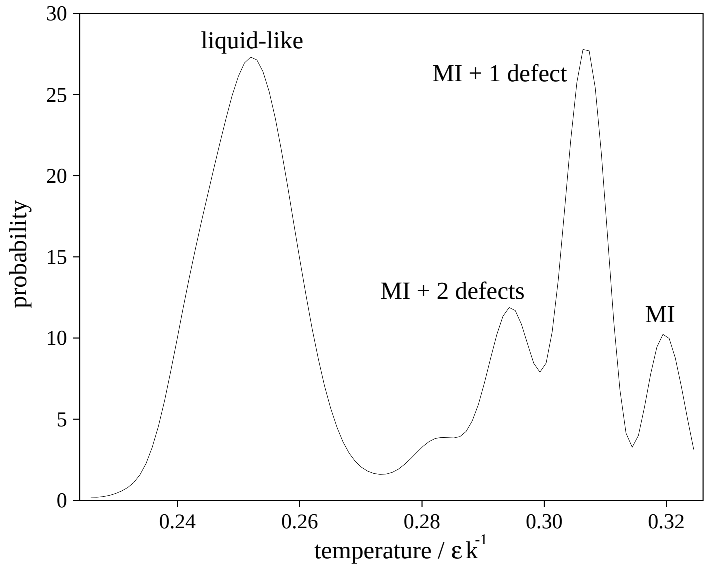

FIGURE 4.13: An example of a multimodal short time-averaged temperature distribution. It is from an MD run for M_{55} at $\rho_0 = 6$ at an energy of $-3.483\,\epsilon\,\mathrm{atom}^{-1}$. Each temperature peak is labelled with the structure associated with it. MI stands for Mackay icosahedron. The averaging period is 3000 time steps.

shown in Figure 4.14. At ρ_0=6, the melting behaviour is very similar to that seen for LJ_{55} in §3.3. The caloric curve has a Van der Waals loop, and surface defects of the Mackay icosahedron can be generated at energies just below that required for complete melting. In comparison, the ρ_0=9 caloric curve shows a higher melting temperature, a deeper S-bend and a greater role for the defective states. This is a direct result of the increasing energy gap between the Mackay icosahedron and the 'liquid-like' band of minima noted in §4.3. At ρ_0=4, the melting temperature is lower than for ρ_0=6, the latent heat is smaller and defective Mackay icosahedra are not seen. Again this can be related to the correlation diagram Figure 4.4 and is simply a result of the decrease in the energy gap between the Mackay icosahedron and the 'liquid-like' band of minima as ρ_0 is decreased.

The behaviour at ρ_0=3 and 13 is significantly different; in particular the melting transitions are closer to a continuous transition than a two-state transition, i.e. between a liquid and a solid. At $\rho_0 = 3$, the lowest energy minimum that we have found is 55A. This minimum lies at the bottom of the band of 'liquid-like' minima, which is approximately continuous in energy. At low temperatures transitions from 55A to higher energy minima begin to occur, because of the small differences in energy. This leads to the fluxional liquid-like behaviour which is exhibited in the rise in Lindemann's δ (Figure 4.14a). Melting occurs at low temperatures without

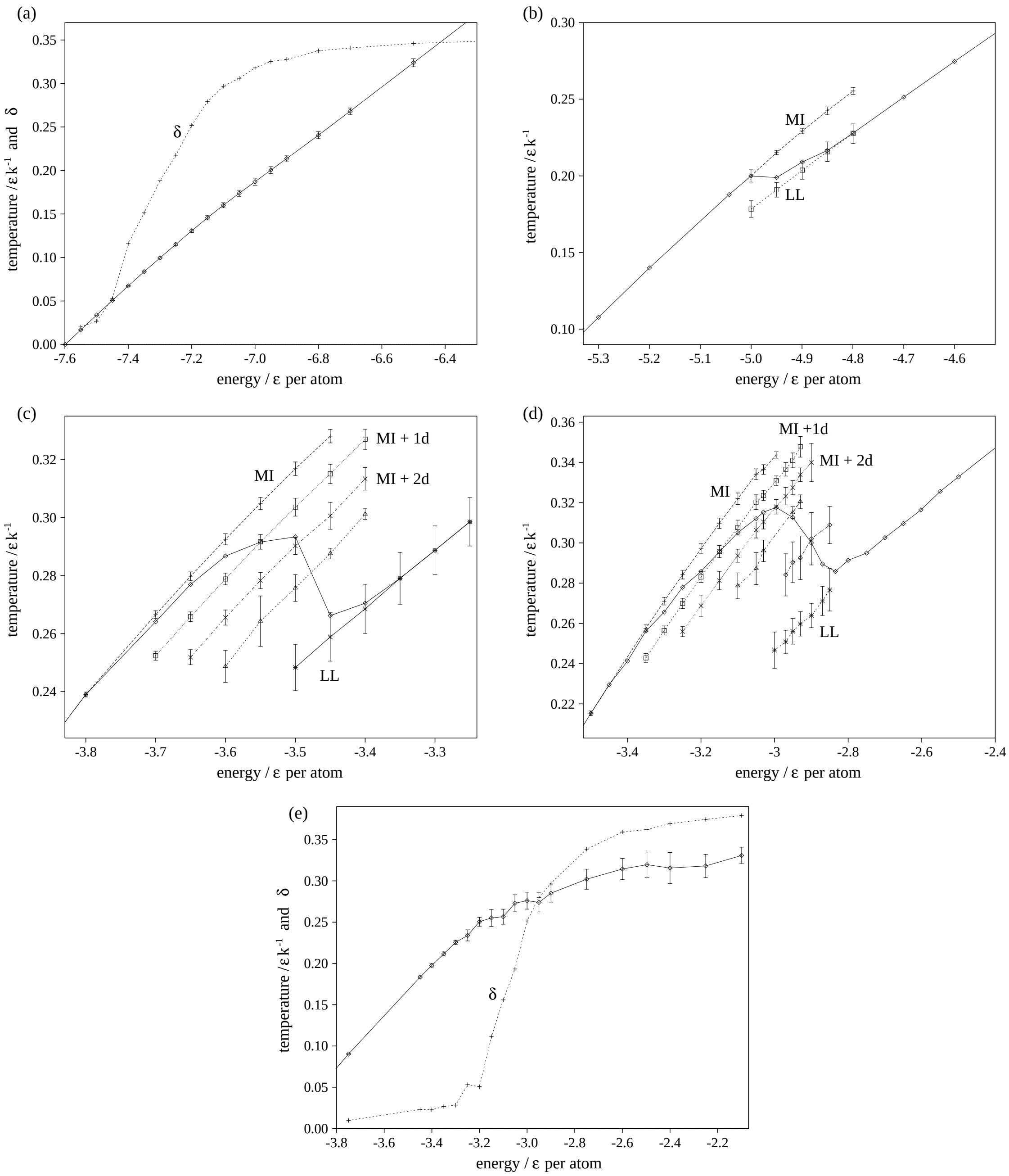

FIGURE 4.14: Caloric curves for M_{55} for ρ_0 = (a) 3, (b) 4, (c) 6, (d) 9 and (e) 13. For ρ_0=3 and 13 Lindemann's δ has also been plotted, so that the melting region can be identified. For ρ_0=4, 6 and 9 the solid line without error bars is the overall caloric curve, and the dashed lines with error bars are the average values of the temperature for the peaks in the STA temperature distribution. The latter lines are labelled with the structures associated with them. MI stands for Mackay icosahedron, + nd for a structure with n defects, and LL for liquid-like.

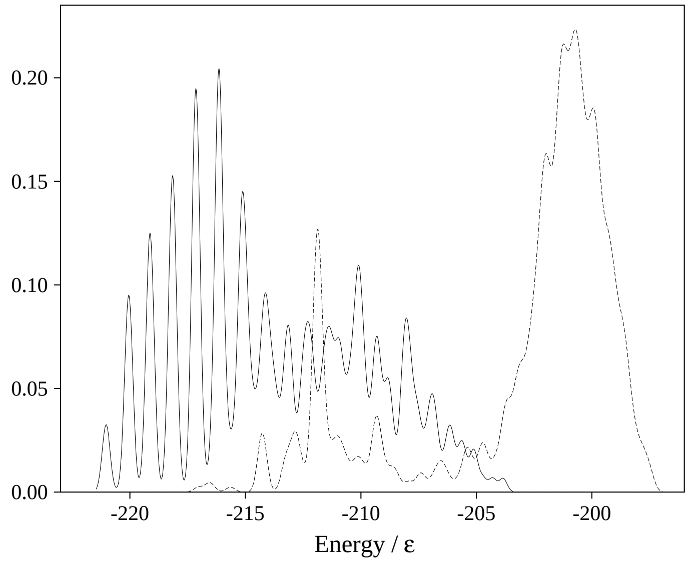

Figure 4.15: Probability distributions of the potential energy for samples of minima for M_{55} at ρ_0=13. The solid line is for a sample of 357 minima obtained by quenching from simulations performed for ρ_0 =13 at energies below $-2.7\epsilon\,\text{atom}^{-1}$. The dashed line is for the ρ_0 =6 sample of minima after reoptimization at ρ_0 =13.

producing any noticeable feature in the caloric curve—the latent heat is essentially zero.

For ρ_0=13, on the other hand, the global minimum is the decahedral structure 55C. The difference in energy between this structure and the 'liquid-like' band of minima is now so large that a transition to the latter is only observed at the highest energies ($E \geq -2.4\epsilon\,\text{atom}^{-1}$) probed by our simulation. This transition occurs after δ has risen to a value which indicates that the cluster has already melted, and does not lead to a noticeable feature in the caloric curve. Instead, as energy is added to 55C, the cluster progresses up a ladder of increasingly defective structures (Figure 4.15—the minima bunch into bands that have the same number of nearest neighbours). This climbing up the PES leads to the decreased slope of the caloric curve at higher energies. The melting transition is quasicontinuous and mediated by defect motion. Defective states of 55C are observed at a lower temperature than the defective states of the Mackay icosahedron in the simulations at ρ_0=6 and 9 simply because the energy gap between the icosahedron and its defective states is larger; the first defective state of the icosahedron has three fewer nearest-neighbour contacts whereas the first defective state of 55C has one less contact[71].

The dependence of the thermodynamic behaviour of M_{55} on its energetic distribution of minima agrees very well with that predicted in a seminal paper by Bixon and Jortner[152], which elucidated this relationship for model PES's. In particular, these authors predicted that significant features in the caloric curve, such as an S-bend, would only be seen when there is a large energy gap between the solid and liquid states (e.g. ρ_0=4, 6 and 9), and not when the energetic distribution of minima is quasi-continuous (e.g. ρ_0=3 and 13).

4.6 Electronic vs Geometric Magic Numbers

Magic numbers based on electronic shells were first observed in mass spectra of alkali metal clusters[214]. These features are now well understood in the framework of the self-consistent spherical jellium model, in which the nearly-free valence electrons are assumed to move in a homogeneous spherical ionic background. Further refinements, such as allowing the cluster to deform into an ellipsoidal shape for incomplete electronic shells, improve the agreement with experiment[94].

In experiments on large sodium clusters by Martin *et al.* electronic shell structure was found to persist up to about 1000 atoms and above this size geometric magic numbers were observed[53]. These magic numbers are associated with the completion of shells of the Mackay icosahedron. Further temperature-dependent experiments have shown that for $N > 1000$ the geometric magic numbers disappear as the temperature is increased[215]. This has been attributed to the loss of icosahedral structure on melting (or surface melting) of the cluster and so has been used to examine the size dependence of the melting temperature. At sufficiently high temperatures, electronic magic numbers have been observed up to at least 3000 sodium atoms[216]. Similarly, experiments on large aluminium clusters have shown that as the temperature is increased the observed magic numbers change from geometric (due to octahedra[217]) to electronic[218].

The natural interpretation of these experiments is that geometric magic numbers are associated with solid-like clusters that are based on a regular packing and that electronic magic numbers are associated with liquid-like clusters. However, before this conclusion can be confirmed, another question must be addressed: could a regularly-packed structure also have the observed electronic shell structure? This has been examined in calculations by Mansikka-aho *et al.* which have shown that the electronic shell structure differs from that observed experimentally for all the common cluster shapes except the icosahedron[219,220]. The icosahedron is sufficiently spherical that the electronic shell structure is similar to the experimental up to 1000 atoms. However, Pavloff and Creagh[221] have shown that the electronic supershell structure observed for sodium clusters[216] cannot be explained if the clusters have icosahedral structure, thus confirming that the sodium clusters which exhibit electronic magic numbers are liquid-like.

Our results allow us to explain the transition. For small Morse clusters with a long-ranged potential the lowest energy minimum has an amorphous structure typical of the liquid-like state. At these sizes, the cluster has a very low melting point, as shown in §4.5, because the lowest energy minimum lies at the bottom of a band of minima which are almost continuous in energy. Hence, the cluster can adopt structures that give the most favourable electronic energy without incurring excessive strain energy and the cluster would be expected to exhibit electronic magic numbers at all temperatures. The effect of size on the correlation diagram is to displace the 'liquid-like' band of minima upwards with respect to the line of the Mackay icosahedron until in the bulk limit regular structures are the lowest in energy for all ρ_0. Increasing the size has an effect similar to decreasing the range of the potential—they both destabilize more strained structures. A corollary of this is the well-known increase in cluster melting temperature with size[222] that was first predicted by Pawlow[223]. As a consequence of this effect, for clusters with long-ranged potentials, there must be a critical size at which the Mackay icosahedron becomes lower in energy than the 'liquid-like' minima. Above this size the cluster would be expected to exhibit geometric shell structure at temperatures below the melting point.

One alternative explanation for this transition that has been proposed by Stampfli and Bennemann simply considers the size- and temperature-dependence of the variation in the electronic and geometric effects[224,225]; they show that the latter is likely to dominate at large sizes. However, in their model they do not include the possibility that small clusters may never adopt regular structures.

The jellium-type models can provide a good description of the alkali metals because these elements most closely approximate free electron systems, and understanding the electronic effects becomes more difficult as one goes further from this limit. Our results lead us to expect that for metals with shorter-ranged potentials geometric magic numbers could be seen at much smaller sizes than for sodium. This may provide an explanation for the behaviour of group II metals: barium clusters of less than 50 atoms show magic numbers consistent with an icosahedral growth sequence[99] and magnesium[54] and calcium[55] have magic numbers due to Mackay icosahedra from 147 atoms upwards. However, it is hard to judge the role many-body forces may play in the energetic competition between regular and disordered structures in these systems.